Desalination and Water Treatment
www.deswater.com
doi: 10.1080/19443994.2014.940218

55 (2015) 2951–2961
September

Taylor & Francis
Taylor & Francis Group

Synthesis of nanocomposite membranes and their application in photocatalytic process for organic pollutions removal from groundwater, East Nile Delta, Egypt

Moustafa M. Abo El-Fadl*, Abdel Hameed M. El-Aassar, Amr A. Mohamed

Hydrogeochemistry Department, Desert Research Center, Cairo, Egypt, Tel./Fax: +202 26389069; email: mmaboelfadl@hotmail.com (M.M. Abo El-Fadl)

Received 14 January 2014; Accepted 16 June 2014

ABSTRACT

Novel sodium alginate (SA)/titanium dioxide (TiO_2) nanocomposite membranes were synthesized using dry casting method as a preparation technique with $CaCl_2$, $BaCl_2$, phosphoric acid, and glutaraldehyde (GA) were tested, as crosslinkers. It was found that GA was the best crosslinker because it gives the best mechanically stable hydrogels, which is not degradable in water. The chemical stability of synthesized membranes was studied at wide pH range from 3 to 13. Also, the characterizations were examined using FTIR spectroscopy, X-ray Diffraction, and Tapping Mode-Atomic Force Microscopy. The applicability of these synthesized membranes as photocatalyst was studied using textile azo-dye methyl orange (MO) as target pollutant. The effects of time, nanoparticles concentration, initial dye concentration, and pH on photocatalysis efficiency of the nanocomposite membranes were investigated through determination of photo-bleaching rate of MO. SA/TiO_2 nanocomposite showed enhanced photocatalytic degradability using optimum operation conditions and can be used in photocatalytic process for organic pollutions removal from groundwater collected from East Nile delta, Egypt.

Keywords: SA/TiO_2; Synthesis; Characterization; Photocatalysis; Organic pollution

1. Introduction

Titanium dioxide (TiO_2) photocatalytic oxidation has received considerable attention as a novel advanced oxidation processes (AOPs) and considered as a promising technology for the disinfection and detoxification of water and wastewater. When catalytic semiconductor powders, such as TiO_2 are suspended in water and irradiated with light ($\lambda < 385$ nm), hydroxyl radicals ($OH^{\cdot}$) and other oxidative species like H_2O_2 and superoxide radicals ($O_2^{\cdot-}$) are generated. The $OH^{\cdot}$ radical is highly toxic towards micro-organisms and very reactive in the oxidation of organic substances [1–6].

SA is a sodium salt of alginic acid, a naturally occurring non toxic polysaccharide found in brown algae. Alginate has been widely used as food and pharmaceutical additive, such as a tablet disintegrate and gelling agent. It contains two uronic acids, α-L-guluronic and

*Corresponding author.

Presented at the Conference on Desalination for the Environment: Clean Water and Energy 11–15 May 2014, Limassol, Cyprus

β-D-mannuronic acids, and is composed of homo-polymeric blocks and blocks with an alternating sequence [7]. It has been reported that SA can be crosslinked with glutaraldehyde (GA), the chemical reaction between hydroxyl groups of SA and GA was confirmed by (FTIR) measurements; thus formed membrane was used in different applications such as the pervaporation separation of organic–organic mixtures [8].

Several studies have demonstrated that the combination of membrane and suspended TiO_2 can help in reducing membrane fouling significantly. Lee et al. [9] indicated that photocatalysis could prevent contaminants from adhering to the membrane surface, and thus decreasing membrane fouling. Xi and Geissen [10] reported that they were able to separate TiO_2 nanoparticles by microfiltration membrane. But in their studies, photocatalysis and membrane separation are two independent operation processes. After photocatalytic reaction, extra membrane filtration must be performed to separate and recover fine TiO_2 powder photocatalyst. This approach may increase the operational complexity and cost in practicable application.

Immobilization of TiO_2 photocatalyst on membrane surface is possibly a reliable approach that may eliminate not only the difficulties in TiO_2 photocatalyst separation, but also could integrate separation and photocatalytic degradation of contaminants in a single membrane device. Anderson and co-workers [11,12] investigated the pioneering possibility of direct coupling membrane separation and photocatalyzed reaction with the use of TiO_2 photocatalytic membranes. Since then, many other researchers were able to fabricate TiO_2 immobilized membranes, on both organic [13–15] and inorganic membranes substrates [16–18].

This work is mainly dealing with the attempt to solve the problem of high concentration of organic pollutants in surface and/or groundwater in the area of East Nile Delta, Egypt using AOPs (Photocatalytic oxidation) with synthesized SA-TiO_2 nanocomposite membranes.

2. Experimental

2.1. Materials and chemicals

- SA, (BDH), England.
- GA (solution 50%): pure reagent for analysis, El-Nasar pharmaceutical chemical Co., Cairo, Egypt.
- Methyl orange (MO): May and Baker LTD Dagenham England.
- TiO_2: P-25 (Evonik), 65 Challenger RD, Ridgefield NJ, US.
- Solvents and inorganic salts were reagent grade and used without further purification.

2.2. Apparatus and methods

2.2.1. Synthesis of membranes

Casting polymer solutions were freshly prepared just before use. SA was dissolved by vigorous stirring in distilled water with or without TiO_2 nanoparticles. The solution was casted on glass plate. The membrane was allowed to dry at different temperature (40, 60, and 80˚C); the best temperature is 60˚C. After drying, batch crosslinking was carried out with 2% GA acidic solution of acetone: water (75:25) mixture.

2.2.2. Photocatalytic experiments

Photocatalytic reaction was carried out in a 250 ml Pyrex glass beaker attached to a 15 W mercury lamp as UV light source with wavelength 254 nm, and the distance between the top of the Pyrex glass beaker and the UV lamp is 5 cm and the light intensity is about 2.33 W/cm^2. The photocatalytic activities of samples were evaluated by measuring the degradation rate of MO solution after a regular interval UV light irradiation. The steps were as follow:

Two hundred milliliter of MO solution with a concentration of 20 ppm and 0.85 g of synthesized membranes with or without doped TiO_2 were introduced into the Pyrex glass beaker at pH 6, the solution was allowed to stand for 60 min before UV irradiation to reach absorption equilibrium due to the difference between MO concentration in the solution and inside of membranes. The degradation rate of MO solution was calculated by the following formula.

$$D = \frac{C_0 - C}{C_0} \times 100\% = \frac{A_0 - A}{A_0} \times 100\% \quad (1)$$

where D is degradation rate, C_0, A_0 and C, A are the concentration and absorbance of MO solution at the absorption peak, 464 nm in adsorption equilibrium before and after UV irradiation, respectively.

2.3. Characterization of synthesized membranes

2.3.1. FT-IR spectroscopy

Analysis by Infrared spectrophotometer was carried out by using Gensis Unicam FT-IR spectrophotometer,

USA. The dimensions of the window to which the film was fixed, were 1.5 × 3 cm.

2.3.2. X-ray diffraction

The X-ray (XRD) diffraction patterns of membranes were measured with Philips Model pw 3710 XRD instrument, Netherlands.

2.3.3. Atomic force microscopy

Atomic force microscopy (AFM) has been performed mainly in tapping mode at room temperature with a Nanoscope V, England. Scanning Probe Imaging Process (SPIP) software was used for analyzing the AFM topographic images.

2.3.4. UV/visible spectrophotometer, Unicam, model 300, England

To determine the suitable wave length for measuring the absorption of the MO dechlorination indication to degradation of total organic mater (TOM).

2.3.5. Conversion and water insoluble

The conversion and water insoluble part (gelation) and swelling% for all resultant membranes were measured as indication of insoluble SA in water%.

The swelling% of the obtained membranes was measured by immersing the known weight membrane samples into water at room temperature (25°C). After an adequate time (3 h) the membrane samples were removed from water and after wiping with a cleaning tissue, they re-weighted. The swelling, conversion, and gelation% were calculated by the following equations:

$$\text{Swelling}\% = \frac{W_{\text{wet}} - W_{\text{dry}}}{W_{\text{dry}}} \times 100$$

$$\text{Conversion}\% = \frac{W_{\text{dry}}}{W_0} \times 100$$

$$\text{Water insoluble part}\% = \frac{W_{\text{dry hot}}}{W_0} \times 100$$

where; W_0 is the weight of the resultant dry membrane, W_{dry} is the weight of the resultant dry membrane after immersion in water at room temperature, $W_{\text{dry hot}}$ is the weight of the resultant dry membrane after immersion in water at 50°C, and W_{wet} is the weight of wet membrane.

2.3.6. Mechanical measurements

Mechanical measurements were carried out by the determination of both tensile strength and elongation%, using an Instron (model-1195-England).

3. Result and discussion

3.1. Synthesis of membranes

3.1.1. Synthesis of SA membranes

All synthesized membranes were basically prepared by the dry casting method using chemical crosslinker. The optimum conditions at which the synthesis and crosslinking processes proceeded successfully were investigated through studying the effect of different parameters on swelling, conversion, and gelation (%). Such parameters were polymer concentration, crosslinker type, impregnation time in crosslinker solution, TiO_2 nanoparticles concentration … etc. as follows.

3.1.1.1. Effect of concentration of sodium alginate. Different concentrations ranged from 2 to 4 wt.% of sodium alginate (SA) were tested. It was found that the best polymer concentration for forming the membrane was 4 wt.% (Table 1). From this table, the swelling% increases with the concentration of SA due to increases of functional groups of OH to form the hydrogen bonds. On the other hand, it gives good mechanical and flexibility properties than other concentrations.

3.1.1.2. Effect of type of crosslinker. Crosslinking is a bond formed between polymer chains, either between different chains or between different parts of the same chain. In our study, $CaCl_2$, $BaCl_2$, phosphoric acid, and GA were tested, as crosslinkers. It was found that GA was the best crosslinker, because it gives the best mechanically stable hydrogels, which is not degradable in water.

Mechanism of crosslinking of SA with GA was suggested as Schema 1. It showed that the two hydroxyl group (OH) of SA polymer reacts with the aldehydic group (CHO) of GA to form crosslinks between the SA chains [19].

Table 1
Effect of concentration of SA

SA conc. (wt.%)	Swelling%	Conversion%	Gelation%
2	34	92	80
3	47	94	90
4	55	93	87

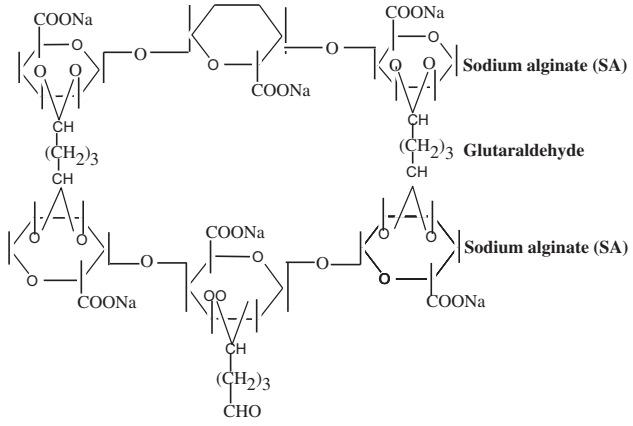

Schema 1. The model structure of crosslinked SA with GA [19].

3.1.1.3. Effect of crosslinker concentration. The concentration of crosslinker is a crucial factor, because the GA is linked through the OH functional groups in the GA. Thus, it decreases numbers of these functional groups. Different concentrations of 1.5, 2, 2.5, and 3 vol.% of GA were trailed to reach the optimum conditions. The results are given in Table 2, it showed that, the increase in crosslinker (%) increase in conversation% and gelation% with decrease in swelling%. So, 2 vol.% of GA gives high swelling% and high conversion% and gelation%.

3.1.1.4. Effect of evaporation temperature. The stability of SA membrane evaporated at different temperature 40, 60, and 80°C are studied. The results are listed in Table 3 and show the suitable temperature is 60°C, this related to the swelling%, conversion%, and gelation% is increased.

3.1.1.5. Effect of impregnation time on the crosslinking process. Different impregnation time used in the crosslinking process is investigated. The results obtained showed that the best time for making the membrane is 18 h, Table 4. Best results were obtained after 18 h. The time gives best result due to the high swelling% and stability of the SA in conversion and gelation (%); this is due to the choice to form more crosslinked SA with GA.

Table 3
Effect of evaporation temperature

Evaporation temp. (°C)	Swelling%	Conversion%	Gelation%
40	37	95	95
60	36	96	94
80	35	97	96

Table 4
Effect of impregnation time on the crosslinking process

Impregnation time (h)	Swelling%	Conversion%	Gelation%
12	39	93	92
18	36	96	94
24	34	95	94

3.1.2. Synthesis of SA/TiO_2 nanocomposite membranes

Optimum conditions for the synthesis of SA membranes were applied. The modification of SA membranes by nano-TiO_2 for use photo degradation of organic pollutions was investigation. SA/TiO_2 nanocomposite membranes were prepared using dry casting method. The optimum conditions of SA membranes were used with mixed TiO_2 nanoparticles. The effect of concentration of nanoparticles onto swelling, conversion, and gelation (%) was studied.

3.1.2.1. Effect of concentration of TiO_2 nanoparticles. Different concentration of TiO_2 nanoparticles of 0.5, 1, 2, and 4 wt.% of the SA concentration were used to investigate the optimum concentration of nanoparticles, Table 5. From the obtained results, 2 wt.% of SA gave higher conversion and best results of swelling and gelation%.

Table 2
Effect of crosslinker concentration

Crosslinker conc. (vol.%)/w of SA	Swelling%	Conversion%	Gelation%
1.5	39	95	94
2.0	36	96	94
2.5	35	96	95
3.0	34	97	96

Table 5
Effect of concentration of TiO_2 nanoparticles

Concentration of TiO_2 (wt.%)	Swelling%	Conversion%	Gelation%
0.5	53	96	94
1	51	93	92
2	46	93	91
4	45	94	93

3.2. Characterization of the synthesized membranes

3.2.1. Effect of pH

The stability of synthesized membranes was studied at different pH ranged between 1 and 13, to investigate the stability of membranes. All synthesized membranes are stable at pH from 1 to 12, where a weight loss less than 10% is observed, while at pH 13 the membrane dissolved, Fig. 1.

3.2.2. FTIR spectroscopy

3.2.2.1. For SA synthesized membranes. Fig. 2 showed the absorption bands of the crosslinked and non crosslinked SA. The main characteristic bands are listed in Table 6.

3.2.2.2. For SA/TiO_2 synthesized membranes. The FTIR spectra of SA/TiO_2 membranes are given in Fig. 3. It showed a metal oxide (TiO_2) characterized bands at 663 cm^{-1} in (SA/0.5%TiO_2), 662 in (SA/2%TiO_2), and 2,852 cm^{-1} of hydroxyl band for surface TiO_2-OH functional group, these results were in agreement with the previous work [20]. The band of OH functional group of crosslinked SA is shifted from 3,425 to 3,403 cm^{-1} for (SA/0.5%TiO_2) and 3,406 cm^{-1} for (SA/2%TiO_2).

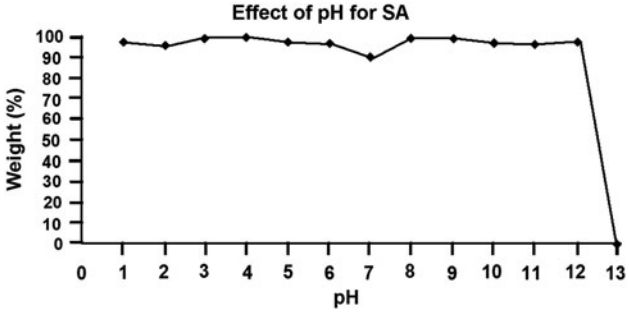

Fig. 1. Effect of pH on the 4 wt.% SA membrane.

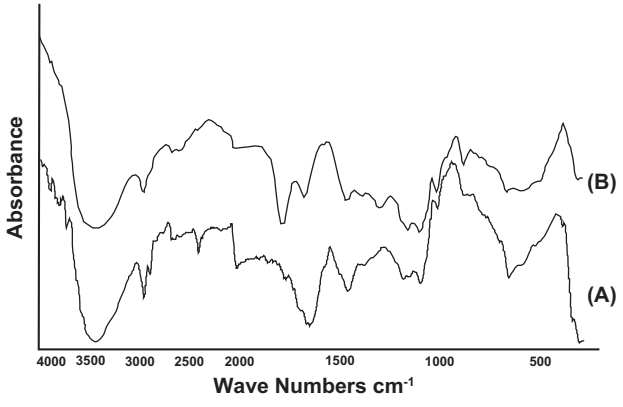

Fig. 2. FTIR Spectra for; (A) non crosslinked SA and (B) crosslinked SA with GA.

3.2.3. XRD patterns

XRD was used to investigate the change in crystallinity of SA that may occur by crosslinking with GA with or without TiO_2 nanoparticles, as shown in Figs. 4 and 5. The degree of crystallinity is the ratio of crystalline and non crystalline components.

Fig. 4 showed that non crosslinked SA exhibit an amorphous character and there is broad peak band at $2\theta = 15^{\circ}$. By crosslinking SA with GA, the nature became more crystalline. Two sharp peaks can be seen at $2\theta = 14$ and 17°.

The XRD of SA/TiO_2 nanocomposite membranes are shown in Fig. 5. It showed peaks of crosslinked SA separated from the peaks of TiO_2 nanoparticles referring to physical bond between them and TiO_2 incorporated in the SA. Whereas in case of SA/$(0.5\%\ TiO_2)_{0.5}$ there are three characteristic peaks of TiO_2 nanoparticles at $2\theta = 25$, 41, and 62°, and in case of SA/(1%TiO_2) there are four peaks characteristic for TiO_2 nanoparticles at $2\theta = 25$, 36, 48, and 62°, but for the SA/(2%TiO_2) there are six peaks characteristic for TiO_2 nanoparticles at $2\theta = 25$, 27, 38, 47, 53, and 62°. This refers to the increasing the number of peaks with increasing the amount of TiO_2 in composites. It should be mentioned here that the intensity of TiO_2 characteristic peaks for anatase at $2\theta = 25.4^{\circ}$ increases with increasing the amount of TiO_2 loaded on SA.

3.2.4. AFM observation

The surface topography of synthesized membranes was studied using tapping mode AFM, the obtained 3D AFM images are shown in Fig. 6.

AFM observations using SPIP software image analysis concerned with the roughness parameters to investigate the correlation between membrane composition and surface properties, Table 7.

The SPIP software allows quantitative determination of roughness parameters by use of the obtained images. The results show the increase of roughness according to (SA/2%TiO_2) > (SA/0.5%TiO_2) > SA which means an increase in the roughness and the surface area by increasing the TiO_2 concentration.

3.3. Photocatalytic activity

The degradation of MO using different synthesized SA, SA/TiO_2 membranes was studied to investigate

Table 6
The main characteristic band of functional groups of SA powder and SA cross linked

Bands assignments	SA powder	SA cross-linked
O–H band stretching	3,442, 3,733, 3,780, 3,802, 3,842, and 3,890 cm^{-1}	3,425 cm^{-1}
C–H stretching bond	2,926 cm^{-1}	2,929 cm^{-1}
O–C=O asymmetric	1,615 cm^{-1}	1,631 cm^{-1}
O–C=O symmetric	1,411 cm^{-1}	1,408 cm^{-1}
C–O–C stretching bond	1,032 cm^{-1}	1,033 cm^{-1}
C=O stretching bond	1,731 cm^{-1}	1,741 cm^{-1}
C–O attributed to its saccharine structure	945 cm^{-1}	941 cm^{-1}
C–O stretching bond	1,032,1,332, and 945 cm^{-1}	1,094,1,333, and 941 cm^{-1}
C–C stretching bond	1,123 cm^{-1}	1,234 cm^{-1}
Characteristic peak of SA (Na–O)	778 cm^{-1}	803 cm^{-1}

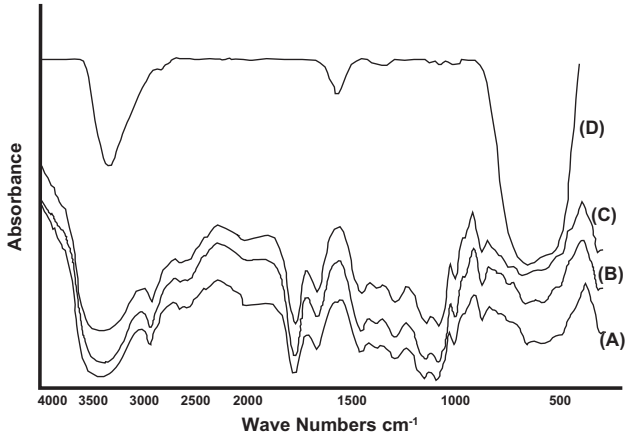

Fig. 3. FTIR Spectra for; (A) SA crosslinked with GA (B) (SA/.5%TiO_2), (C) (SA/2%TiO_2), and (D) TiO_2 powder.

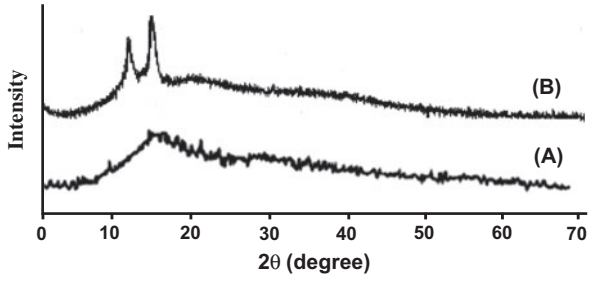

Fig. 4. XRD for; (A) SA powder and (B) SA crosslinked GA.

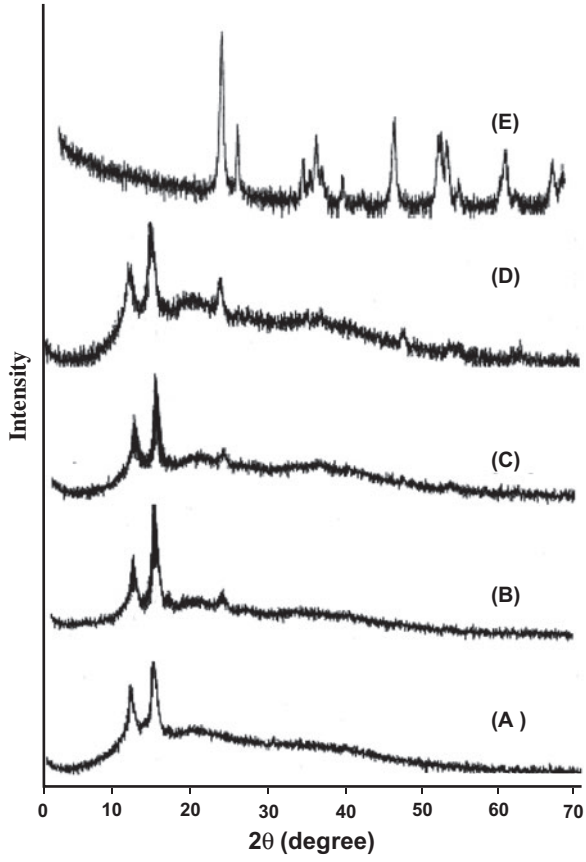

Fig. 5. XRD for; (A) SA crosslinked SA (B) SA/(0.5%TiO_2) (C) SA/(1%TiO_2) (D) SA/(2%TiO_2) (E) TiO_2.

the activity of nanocomposite membranes for degradation of organic pollutant under UV radiation. The study was performed at optimum UV wavelength, pH ranged from 3 to 10, dye concentrations of 10, 20, and 30 ppm and different concentrations of SA/TiO_2. All the experiments were done at room temperature (27 ± 2°C). The molecular structure of MO is shown in Schema 2.

The optimum wavelength for measuring the absorbance of the MO decolorization with time is shown in Fig. 7. It shows that the optimum wavelength for measuring the absorbance of MO decolorization with time

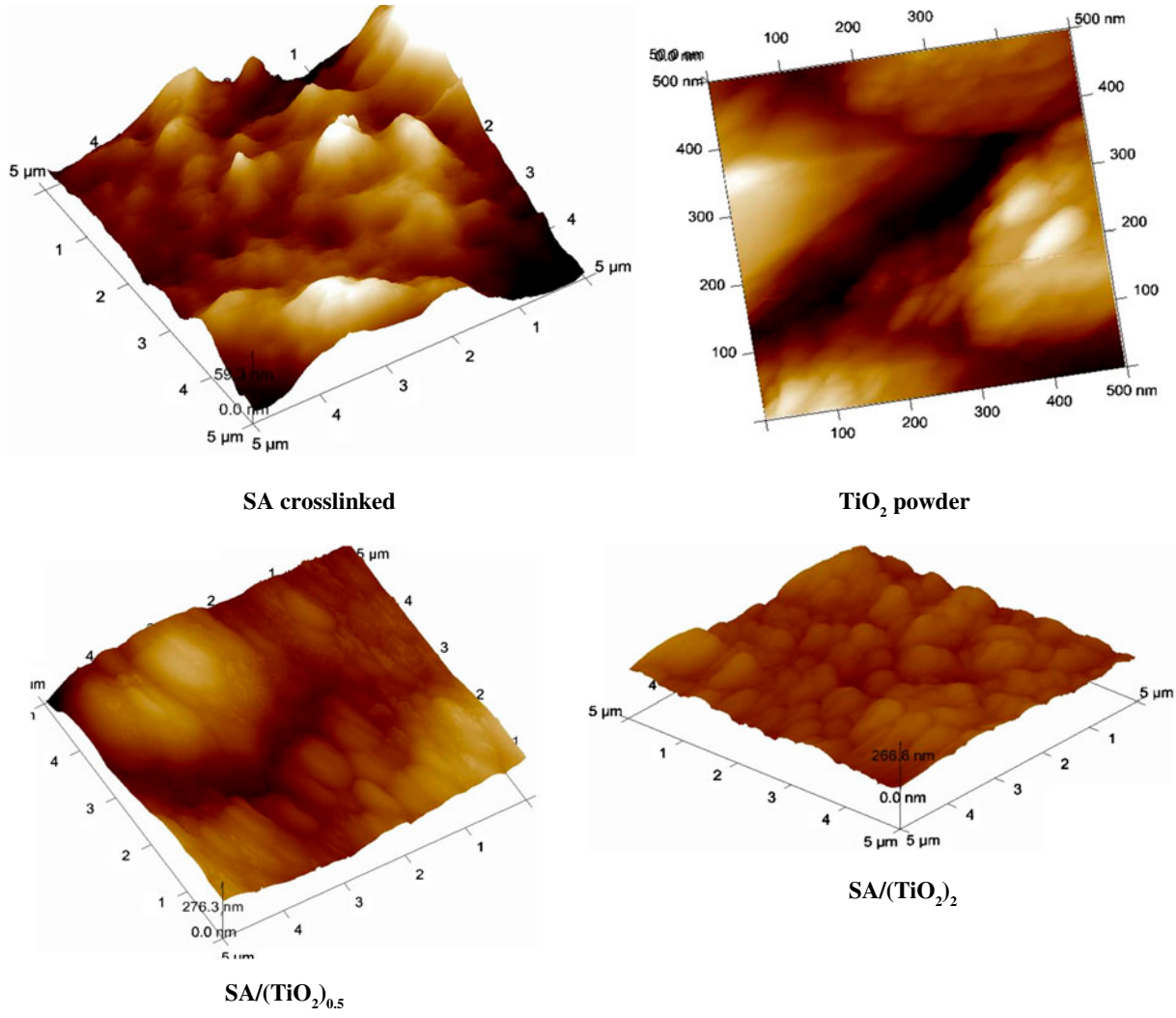

Fig. 6. 3D image of crosslinked SA, TiO_2 powder, SA/(0.5%TiO_2), and SA/(2%TiO_2).

at pH 3.5 equal 506 nm, but for pH 7 and 10 the optimum wavelength is 464 nm. Seven milliliters of sample were performed at interval of 15 min in continuous 2.25 h. The photo-degradation efficiency was monitored by measuring the absorbance of the solution samples at its maximum absorption wavelength of 464 nm with UV–vis spectroscopy. The decolorization efficiency as a function of time was calculated by the absorbency values of the original and analytical samples.

In order to study the effect of light on the degradability of MO, control experiments were performed in

Table 7
Surface area roughness of SA, TiO_2 powder, (SA/0.5%TiO_2), and (SA/2%TiO_2)

Type of sample analysis	SA crosslinked	TiO_2 powder	(SA/0.5%TiO_2)	(SA/TiO_2)$_2$
Rq (nm)	21.4	19.2	60	70
Ra (nm)	16.2	15.7	48.5	60
Rm (nm)	152	92.6	392	415

Note: Rq is corresponding to root mean square roughness, Ra is the mean roughness, and Rm is the maximum height.

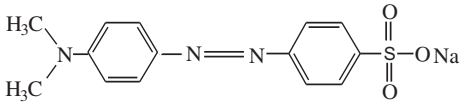

Schema 2. The molecular structure of MO.

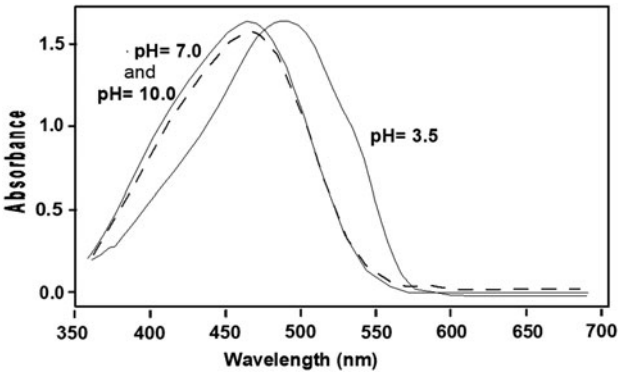

Fig. 7. Electronic absorption spectra of MO (20 ppm) in aqueous solution.

dark and under UV conditions. In dark, the experiment showed that MO on SA/TiO_2 membrane remained stable for 2 h, whereas, under UV light the MO on SA/TiO_2 membrane is degraded 1.73% in 2 h, this is low degradation efficiency. The photo-degradation efficiency was monitored by measuring the absorbance of the solution samples at its maximum absorption wavelength of 464 nm with UV–vis spectroscopy.

3.3.1. Factors affecting the photo-degradation process

3.3.1.1. Effect of time on the degradation of MO dye. The degradation efficiency as a function of time was calculated by the absorbance values of the original and analytical samples. Time of the photo-degradation is an important factor in the photocatalytic process, Fig. 8. It was obvious that 120 min illumination time is the optimum time for the photocatalytic degradation.

3.3.1.2. Effect of nanoparticles concentration. The effect of the concentration of TiO_2 nanoparticles that doped onto SA/TiO_2 nanocomposite membrane on the photocatalytic process was studied, Fig. 9. This figure shows the photo-degradation results at various concentrations of SA/TiO_2 nanocomposite membranes using dye concentration equal to 20 ppm, for 2 h reaction time, at pH 6. It was found that the addition of catalysts enhanced the degradation efficiency.

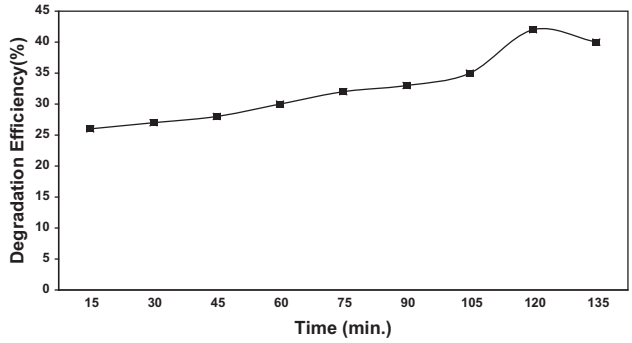

Fig. 8. Effect of time on photo-degradation of MO dye (20 ppm) using $SA/(TiO_2)_2$ at pH 6.

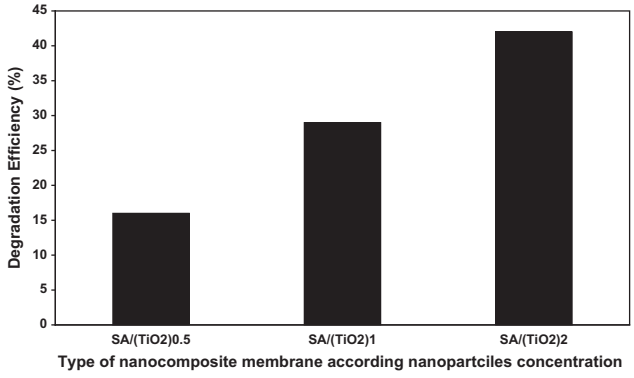

Fig. 9. Effect of TiO_2 nanoparticles different concentration on the photo-degradation efficiency at constant time.

3.3.1.3. Effect of initial dye concentration. The effect of initial MO dye concentration ranged from 10 to 30 ppm on the rate of photo-degradation efficiency (%) was studied using the best $(SA/TiO_2)_2$ nanocomposite membrane at pH 6, as shown in Fig. 10. The results showed a decrease in the degradation efficiency with increasing the concentration of dye, this result is in agreement with the previous work of Kansal et al. [21]. This is attributed to reduced concentration of $OH^{\cdot}$ radicals on the catalyst surface with increasing the concentration of dye [22,23].

3.3.1.4. Effect of pH values. The pH is an important factor in the evaluation of photocatalytic reactions in aqueous solution. The effect of pH was studied by keeping all other experimental conditions constant and changing the initial pH value between 3 and 10. The degradation efficiency was studied on membranes $(SA/TiO_2)_2$ using initial dye concentration of 20 ppm. The results are given in Fig. 11. A decrease in decolorization rate can be seen with increasing pH up to 10.

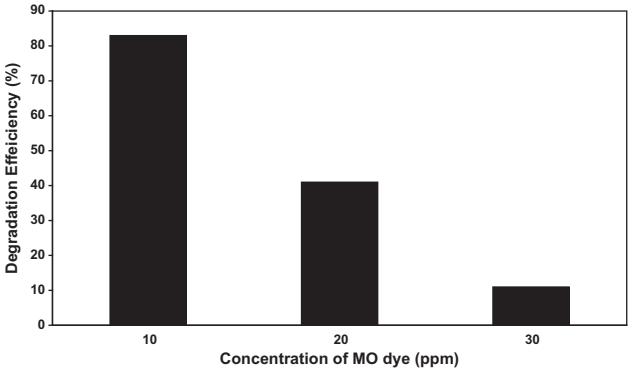

Fig. 10. Effect of initial MO dye concentration on the photo-degradation efficiency.

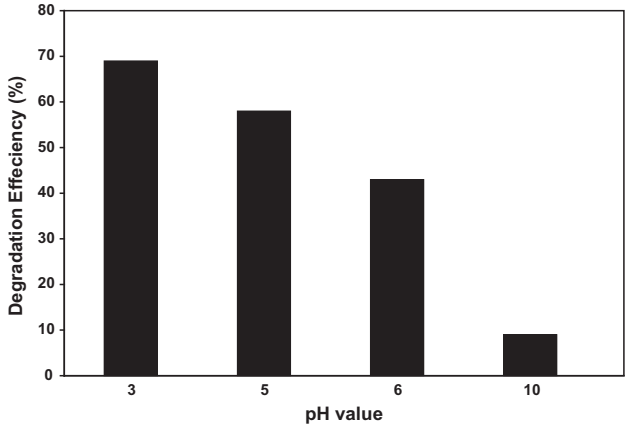

Fig. 11. Effect of pH on the photo-degradation efficiency of (SA/ 2%TiO_2) at constant time.

Higher pH retarded the formation of $OH^{\cdot}$ radicals and decreased the photocatalytic reaction rate [24].

3.3.2. Reusability of $SA/(TiO_2)_2$ nanocomposite membranes

The possibility of recovery and reuse of membrane for photocatalytic degradation is a very important factor in practical applications. The reproducibility of the photocatalytic degradation activity was tested for investigated membranes with a constant MO concentration (20 ppm) and 0.85% membrane catalyst dose $(SA/TiO_2)_2$ for each cycle. The regeneration of the catalyst is done by the following procedure. After the photocatalytic degradation of the MO solution, the membrane was removed and washed with distilled water and dried at 35˚C for 1hr. This recovered SA/TiO_2 nanocomposite membrane was reused in the next cycle. The results obtained are shown in Fig. 12. It is

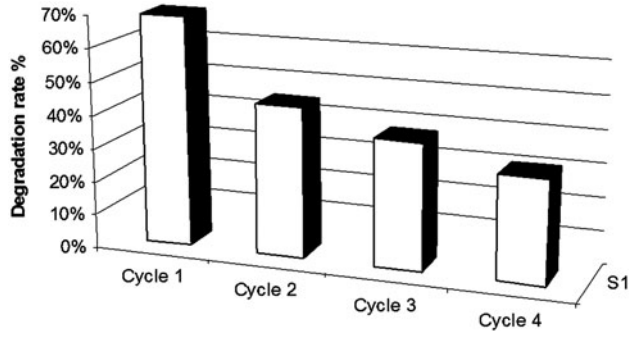

Fig. 12. Reuse of $(SA/TiO_2)_2$ nanocomposite membrane in treatment of polluted water by TOC in study area.

observed that the degradation rate decreases from 68 to 28% after four cycles accompanied by a weight loss of membrane from 6.1 to 8.2%. The doped TiO_2 on the SA nanocomposite membrane could be used for a maximum of four times before it becomes inefficient. This effect is attributed to the deactivation of the catalyst surface by the by-products of degradation of the dye and polymer degradation by the deposited titania [23].

3.3.3. Kinetic study

The kinetics of UV-degradation of MO at concentration of 20 ppm under UV irradiation is illustrated in Fig. 13. The results show that the photocatalytic decolorization of MO dye can be described by the first order kinetic model, $\ln (C_0/C) = kt$, where C_0 is the initial concentration and C is the concentration at time t. The plots of the concentration data gave a straight line. The rate constant was found to be 0.0011 min^{-1} with a correlation factor 0.98. The photocatalytic degradation kinetic indicated that the destruction rate of photocatalytic oxidation of MO dye over illuminated TiO_2 fitted the Langmuir–Hinshelwood (L–H) kinetics model [25,26].

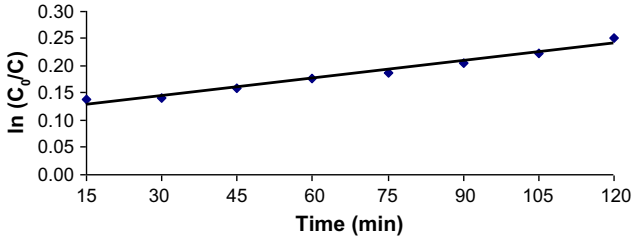

Fig. 13. Pseudo-first-order kinetics for MO photocatalyzed degradation.

Table 8
Photocatalytic degradation of polluted water samples in East Nile Delta area, Egypt

Sample location	TOC before treatment (ppm)	TOC after treatment (ppm)	Efficiency %
Bahr El Baqar	608	347	57
Bahr El Batekh	173.6	Nil	100
El-Salhyia treatment station	126.5	Nil	100

3.3.4. Application of SA/$(TiO_2)_2$ in organic pollutants removal

SA/$(TiO_2)_2$ synthesized membrane was used to study its efficiency in the environmental treatment of total organic carbon (TOC) in natural waters such as Bahr El Baqar, Bahr El Batekh drains, and Discharge of El-Salhyia treatment station. This area is polluted by many contaminants such as COD, BOD, and heavy metals, [27]. The results that were obtained after 2 h are given in Table 8. SA/$(TiO_2)_2$ synthesized membrane shows high efficiency that it can be used efficiency up to 100% in treatment of TOC by used the color methods [28].

4. Conclusions

Novel crosslinked SA/TiO_2 nanocomposite polymer membrane was prepared by a dry casting method. A SA/TiO_2 nanocomposite polymer membrane was synthesized by a dry casting method. The SA/TiO_2 nanocomposite has a favorable adsorption of MO solution, and higher photocatalytic efficiency for decolorization of MO solution under UV irradiation. The SA/TiO_2 nanocomposite can be recovered easily from reaction solution. Therefore, the nanocomposite is hopeful to be used in degradation of organic pollutants. Further investigation is in progress.

References

[1] S.S. Block, V.P. Seng, D.Y. Goswami, Chemically enhanced sunlight for killing bacteria, ASME J. Solar Energy 119 (1997) 85–91.
[2] T. Matsunaga, R. Tomoda, T. Nakajima, H. Wake, Photo-electrochemical sterilization system that uses photosemiconductor powders, FEMS Microbiol. Lett. 29 (1985) 211–214.
[3] C. Wei, W.Y. Lin, Z. Zainal, N.E. Williams, K. Zhu, A.P. Kruzic, R.L. Smith, K. Rajeshwar, Bactericidal activity of TiO_2 photocatalyst in aqueous media: Toward a solar-assisted water disinfection system, Environ. Sci. Technol. 28 (1994) 934–938.
[4] T. Matsunaga, M. Okochi, TiO_2-mediated photochemical disinfection of *Escherichia coli* using optical fibers, Environ. Sci. Technol. 29 (1995) 501–505.
[5] A.G. Rincon, P. Peringer, N. Adler, C. Pulgarin, Interaction between *E. coli* inactivation and DBP precursors-dihydroxy benzene isomers-in the photocatalytic process of drinking water with TiO_2, J. Photochem. Photobiol., A 139 (2001) 233–241.
[6] A.G. Rincón, C. Pulgarin, Photocatalytical inactivation of *E. coli*: Effect of (continuous-intermittent) light intensity and of (suspended-fixed) TiO_2 concentration, Appl. Catal., B 44 (2003) 263–284.
[7] K.I. Draget, Alginates, in: G.O. Philips, P.A. Williams (Eds.), Handbook of Hydrocolloids, Woodhead Publishing Ltd, Cambridge, UK, 2000, pp. 379–395.
[8] C.K. Yeom, K.H. Lee, Characterization of sodium alginate membrane crosslinked with glutaraldehyde in pervaporation separation, J. Appl. Polym. Sci. 67 (1998) 209–219.
[9] S.A. Lee, K.H. Choo, C.H. Lee, H.I. Lee, T.W. Hyeon, W.Y. Choi, H.H. Kwon, Use of ultrafiltration membranes for the separation of TiO_2 photocatalysts in drinking water treatment, Ind. Eng. Chem. Res. 40 (2001) 1712–1719.
[10] W. Xi, S.U. Geissen, Separation of titanium dioxide from photocatalytically treated water by cross-flow microfiltration, Water Res. 35 (2001) 1256–1262.
[11] M.D. Moosemiller, J.R.C.G. Hill, M.A. Anderson, Physicochemical properties of supported γ-Al_2O_3 and TiO_2 ceramic membranes, Sep. Sci. Technol. 24 (1998) 641–657.
[12] M.A. Anderson, M.J. Gieselmann, Q.J. Xu, Titania and alumina ceramic membranes, J. Membr. Sci. 39 (1988) 243–258.
[13] R. Molinari, M. Mungari, E. Drioli, A. Di Paola, V. Loddo, L. Palmisano, M. Schiavello, Study on a photocatalytic membrane reactor for water purification, Catal. Today 55(1–2) (2000) 71–78.
[14] Z.Y. Yu, E. Mielczarski, J. Mielczarski, D. Laub, P. Buffat, U. Klehm, P. Albers, K. Lee, A. Kulik, L. Kiwi-Minsker, A. Renken, J. Kiwi, Preparation, stabilization and characterization of TiO_2 on thin polyethylene films (LDPE): Photocatalytic applications, Water Res. 41 (2007) 862–874.
[15] P. Yang, M. Yang, S. Zou, J. Xie, W. Yang, Positive and negative TiO_2 micro patterns on organic polymer substrates, J. Am. Chem. Soc. 129 (2007) 1541–1552.
[16] U. Aust, S. Benfer, M. Dietze, A. Rost, G. Tomandl, Development of microporous ceramic membranes in the system TiO_2/ZrO_2, J. Membr. Sci. 281 (2006) 463–471.
[17] Ángeles de la Rubia, M. Rodríguez, D. Prats, pH, ionic strength and flow velocity effects on the NOM filtration with TiO_2/ZrO_2 membranes, Sep. Purif. Technol. 52 (2006) 325–331.
[18] T. Van Gestel, B. Van der Bruggen, A. Buekenhoudt, C. Dotremont, J. Luyten, C. Vandecasteele, G. Maes, Surface modification of γ-Al_2O_3/TiO_2 multilayer

membranes for applications in non-polar organic solvents, J. Membr. Sci. 224 (2003) 3–10.
[19] B.V.K. Naidu, K.S.V.K. Rao, T.M. Aminabhavi, Pervaporation separation of water + 1,4-dioxane and water + tetrahydrofuran mixtures using sodium alginate and its blend membranes with hydroxyethyl cellulose—A comparative study, J. Membr. Sci. 260 (2005) 131–141.
[20] Z. Zainal, L.K. Hui, M.Z. Hussein, A.H. Abdullah, I.R. Hamadneh, Characterization of TiO_2-chitosan/glass photocatalyst for the removal of a mono azo dye via photodegradation-adsorption process, J. Hazard. Mater. 164 (2009) 138–145.
[21] S. Kansal, M. Singh, D. Sudc, Studies on photo-degradation of two commercial dyes in aqueous phase using different photo catalysts, J. Hazard. Mater. 141 (2006) 581–590.
[22] I. Poulios, D. Makri, X. Prohaska, Photocatalytic treatment of olive milling waste water: Oxidation of protocatechuic acid, Global NEST: The Int. J. 1 (1999) 55–62.
[23] K. Venkata, S. Roa, M. Subrahmanyam, P. Boule, Immobilized TiO_2 photocatalyst during long-term use: Decrease of its activity, Appl. Catal., B 49 (2004) 239–249.
[24] N.A. Laoufi, D. Tassalit, F. Bentahar, The degradation of phenol in water solution by TiO_2 photocatalysis in a helical reactor, Global NEST J. 10(3) (2008) 404–418.
[25] J. Cunningham, G. Al-Sayyed, S. Srijaranai, Adsorption of model pollutants onto TiO_2 particles in relation to photo-remediation of contaminated water, in: G. Helz, R. Zepp, D. Crosby (Eds.), Aquatic and Surface Photochemistry, Lewis Publications, CRC Press, 1994, pp. 317–348 (Chapter 22).
[26] A. Olivira-Campose, O. Peter, L. Poulios, Photocatalytic degradation studies on malachite green, in: Environment 2010: Situation and perspectives for the European Union 6–10 May 2003, Porto, Portugal, 2003, pp. 1–6.
[27] A.A. Amr, Chemical Studies of Water Resources and Their Treatment for Pollution Control Using Nanotechnology Technique in Some Localities in Eastern Nile Delta – Egypt, Faculty of Science, Benha University, Benha, 2010.
[28] American Society for Testing and Materials, Water and Environmental Technology, Annual Book of ASTM Standards, Sec. 11, vol. 11.01 and 11.02, West Conshohocken, PA, USA, 2002.